

Valley contrasting physics in graphene: magnetic moment and topological transport

Di Xiao,* Wang Yao,* and Qian Niu

Department of Physics, The University of Texas, Austin, TX 78712-0264

(Dated: November 26, 2024)

We investigate physical properties that can be used to distinguish the valley degree of freedom in systems where inversion symmetry is broken, using graphene systems as examples. We show that the pseudospin associated with the valley index of carriers has an intrinsic magnetic moment, in close analogy with the Bohr magneton for the electron spin. There is also a valley dependent Berry phase effect that can result in a valley contrasting Hall transport, with carriers in different valleys turning into opposite directions transverse to an in-plane electric field. These effects can be used to generate and detect valley polarization by magnetic and electric means, forming the basis for the so-called valley-tronics applications.

PACS numbers: 73.63.-b, 75.75.+a, 85.35.-p

Graphene, the monolayer carbon honeycomb lattice, has extraordinary electronic properties [1, 2]. Its band structure has two degenerate and inequivalent valleys at the corners of the Brillouin zone. Because of their large separation in momentum space, inter-valley scattering is strongly suppressed [3, 4], implying the potential use of valley index in a way similar to the role of spin in spintronics applications. Interesting valley dependent phenomena are being actively explored [5].

In this Letter, we propose a general scheme to generate and detect valley polarization in graphene systems with broken inversion symmetry. We reveal that there is an intrinsic magnetic moment associated to the valley index, in close analogy with the Bohr magneton to the electron spin. This property makes the valley polarization a directly measurable physical quantity. The broken inversion symmetry also allows a valley Hall effect, where carriers in different valleys flow to opposite transverse edges when an in-plane electric field is applied. It opens a new possibility to the much desired electric generation and detection of valley polarization. The valley Hall effect is analogous to the spin Hall effect [6], and falls into the same category as the Berry-phase supported topological transport phenomena.

Graphene systems with broken inversion symmetry are of direct experimental relevance. Zhou *et al.* [7] have recently reported the observation of a band gap opening in epitaxial graphene, attributed to the inversion symmetry breaking by the substrate potential. In addition, in biased graphene bilayer, inversion symmetry can be explicitly broken by the applied interlayer voltage [8, 9]. Moreover, as we show below, the emergent valley contrasting physics is a generic consequence of bulk symmetry properties, which provides a new and much standard pathway to potential applications of ‘valleytronics’ in a broad class of semiconductors [10], as compared to the novel valley device relying on the peculiar property of the edge state in graphene nanoribbon [5]. Graphene with broken inversion symmetry serves as a paradigm to demonstrate the general features and necessary conditions of such ap-

plications.

Before starting specific calculations, it will be instructive to make some general symmetry analysis. A valley contrasting magnetic moment has the relation $\mathbf{m}_v = \chi\tau_z$, where $\tau_z = \pm 1$ labels the two valleys and χ is a coefficient characterizing the material. Under time reversal, \mathbf{m}_v changes sign, and so does τ_z (the two valleys switch when the crystal momentum changes sign). Therefore, χ can be non-zero even if the system is non-magnetic. Under spatial inversion, only τ_z changes sign. Therefore \mathbf{m}_v can be nonzero only in systems with broken inversion symmetry.

Inversion symmetry breaking simultaneously allows a valley Hall effect, with $\mathbf{j}^v = \sigma_H^v \hat{z} \times \mathbf{E}$, where σ_H^v is the transport coefficient (valley Hall conductivity), and the valley current \mathbf{j}^v is defined as the average of the valley index times the velocity operator. Under time reversal, both the valley current and electric field are invariant. Under spatial inversion, the valley current is still invariant but the electric field changes sign. Therefore, the valley Hall conductivity can be non-zero when the inversion symmetry is broken, even if the time reversal symmetry remains.

Armed with the insight from the above symmetry analysis, we now consider a concrete example, a single graphene layer with a staggered sublattice potential breaking the inversion symmetry. Staggered sublattice potential is generally expected in epitaxial graphene as pointed out in the review by Geim and Novoselov [2] and explicitly shown by *ab initio* studies [11]. In the tight binding approximation, it can be modeled with a nearest-neighbor hopping energy t and a site energy difference Δ between sublattices [12, 13, 14]. For relatively low doping, we can resort to the low-energy description near the Dirac points. The Hamiltonian is given by

$$H = \frac{\sqrt{3}}{2} at(q_x \tau_z \sigma_x + q_y \sigma_y) + \frac{\Delta}{2} \sigma_z, \quad (1)$$

where σ is the Pauli matrix accounting for the sublattice index, and \mathbf{q} is measured from the valley center

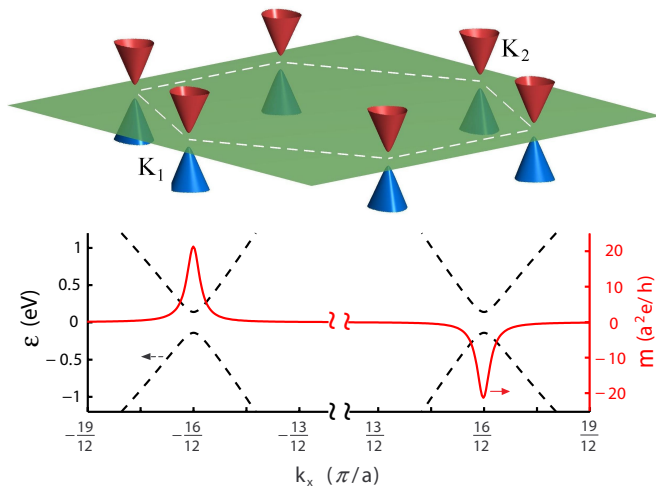


FIG. 1: (color online). Energy bands (top panel) and orbital magnetic moment of the conduction bands (bottom panel) of a graphene sheet with broken inversion symmetry. The Berry curvature $\Omega(\mathbf{k})$ has a distribution similar to that of $\mathbf{m}(\mathbf{k})$. The first Brillouin zone is outlined by the dashed lines, and two inequivalent valleys are labeled as K_1 and K_2 . The top panel shows the conduction (red) and valence (blue) bands in the energy range from -1 to 1 eV. The parameters used are $t = 2.82$ eV and $\Delta = 0.28$ eV.

$\mathbf{K}_{1,2} \equiv (\mp 4\pi/3a)\hat{\mathbf{x}}$ with a being the lattice constant. In the following we shall focus on the n -doped graphene. Generalization to the p -doped graphene is straightforward due to the particle-hole symmetry presented in this system.

Because spin-orbit coupling is extremely weak in graphene [15], the valley magnetic moment can only be of orbital nature. To study this quantity, we invoke the semiclassical formulation of the wavepacket dynamics of Bloch electrons [16]. It has been shown that in addition to the spin magnetic moment, Bloch electrons carry an orbital magnetic moment given by $\mathbf{m}(\mathbf{k}) = -i(e/2\hbar)\langle \nabla_{\mathbf{k}} u | \times [H(\mathbf{k}) - \varepsilon(\mathbf{k})] | \nabla_{\mathbf{k}} u \rangle$, where $|u(\mathbf{k})\rangle$ is the periodic part of the Bloch function, $H(\mathbf{k})$ is the Bloch Hamiltonian, and $\varepsilon(\mathbf{k})$ is the band energy [16]. It originates from the self-rotation of the wavepacket. For a two-dimensional system, the orbital magnetic moment is always in the normal direction of the plane and may be written as $\mathbf{m}(\mathbf{k})\hat{\mathbf{z}}$. Its momentum dependence can easily be calculated from the tight-binding Bloch states, and is shown in Fig. 1. As we can see, $\mathbf{m}(\mathbf{k})$ is concentrated in the valleys and has opposite signs in the two inequivalent valleys. Analytic expression can also be obtained from the model Hamiltonian (1) in the neighborhood of such valleys:

$$\mathbf{m}(\mathbf{k}) = \tau_z \frac{3ea^2\Delta t^2}{4\hbar(\Delta^2 + 3q^2a^2t^2)}. \quad (2)$$

It is instructive to consider the low energy limit ($\mathbf{q} \rightarrow$

0) of the orbital magnetic moment

$$\mathbf{m}(\mathbf{K}_{1,2}) = \tau_z \mu_B^*, \quad \mu_B^* = \frac{e\hbar}{2m_e^*}, \quad (3)$$

where $m_e^* = (2\Delta\hbar^2)/(3a^2t^2)$ is the effective mass at the band bottom. This is in close analogy with the Bohr magneton for the electron spin, where the effective mass becomes the free electron mass. In fact, the analogy goes further, because one can also obtain the spin Bohr magneton by constructing a wavepacket at the bottom of the positive energy bands of the Dirac theory and calculating the self-rotating orbital moment. Therefore, it makes sense to call the orbital moment calculated above as the intrinsic magnetic moment associated with the valley degree of freedom, provided one is only concerned with low energy electrons near the bottom of the valleys [18, 19].

The valley magnetic moment has important implications in valleytronics as it can be inferred from all kinds of experiments analogous to those on the spin magnetic moment. For example, while spin polarization of electrons can be created by a magnetic field (Pauli paramagnetism), we expect a similar valley polarization in graphene due to coupling between a perpendicular magnetic field and the valley magnetic moment. Moreover, for typical values of $\Delta \sim 0.28$ eV and $t \sim 2.82$ eV with a lattice constant $a = 2.46$ Å we find μ_B^* to be about 30 times of the Bohr magneton. Therefore the response to a perpendicular magnetic field is in fact dominated by the valley magnetic moment at low doping in graphene. Interestingly, unlike the spin moment which will respond to magnetic fields in all directions, μ_B^* only couples to magnetic fields in the z -direction. This strong anisotropic magnetic response may be used to distinguish the spin and valley magnetic moment.

Complimentarily, a population difference in the two valleys may be detected as a signal of orbital magnetization. The orbital magnetization consists of the orbital moments of carriers plus a correction from the Berry curvature [20]

$$M = 2 \int \frac{d^2k}{(2\pi)^2} [\mathbf{m}(\mathbf{k}) + (e/\hbar)(\mu - \varepsilon(\mathbf{k}))\Omega(\mathbf{k})], \quad (4)$$

where μ is the local chemical potential, and the integration is over states below the chemical potential. The Berry curvature $\Omega(\mathbf{k}) = \Omega(\mathbf{k})\hat{\mathbf{z}}$ is defined by $\Omega(\mathbf{k}) = \nabla_{\mathbf{k}} \times \langle u(\mathbf{k}) | i \nabla_{\mathbf{k}} | u(\mathbf{k}) \rangle$ and its distribution has a similar structure to that of $\mathbf{m}(\mathbf{k})$. We note that Eq. (4) is for temperatures much lower than the energy scale of band structure (roughly given by Δ), which holds up to room temperature as the experimentally observed bandgap $\Delta \sim 0.28$ eV [7]. For two-band model with particle-hole symmetry, we have a simple relation between the orbital magnetic moment and the Berry curvature in the conduction band: $\mathbf{m}(\mathbf{k}) = (e/\hbar)\varepsilon(\mathbf{k})\Omega(\mathbf{k})$. Using this relation, Eq. (4) may be further simplified as

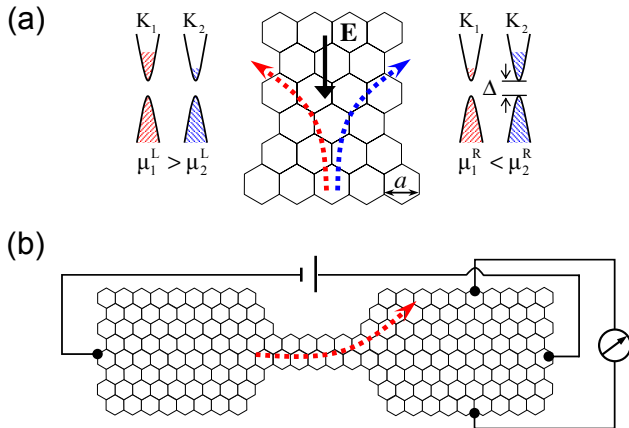


FIG. 2: (color online). Electric generation (a) and detection (b) of the valley polarization. (a) An in-plane electric field will generate a transverse valley current, which leads to a net valley polarization on the sample edges. (b) A valley-polarization created by the valley filter [5] results in a transverse voltage across the sample.

$M = 2(e/\hbar) \int \frac{d^2k}{(2\pi)^2} \mu \Omega(\mathbf{k})$. When the two valleys are in equilibrium (the chemical potential μ is common to both), this integral vanishes because the Berry curvature has opposite values in the two valleys. In the presence of a population difference, the chemical potential has different values in the two valleys $\mu_1 \neq \mu_2$. Therefore, the net orbital magnetization is given by

$$\delta M = 2 \frac{e}{\hbar} [\mu_1 C_1(\mu_1) + \mu_2 C_2(\mu_2)] \approx 2 \frac{e}{\hbar} C_1(\bar{\mu}) \delta \mu, \quad (5)$$

where $2\pi C_i(\mu) = \int^{\mu_i} d^2k \Omega(\mathbf{k})$ is the Berry phase around the Fermi circle in valley K_i , $\delta \mu \equiv \mu_1 - \mu_2$ and $2\bar{\mu} \equiv \mu_1 + \mu_2$. The approximate equality holds for $\mu_i > \Delta$, where the Berry phases approach $\pm\pi$. Thus in a crude estimation, δM reduces to $(e/\hbar)\delta\mu$.

Next we discuss the Berry-phase supported topological transport in our system. It has been well established that in the presence of an in-plane electric field, an electron will acquire an anomalous velocity proportional to the Berry curvature in the transverse direction [16], giving rise to an intrinsic contribution to the Hall conductivity [21, 22], $\sigma_H^{\text{int}} = 2(e^2/\hbar) \int \frac{d^2k}{(2\pi)^2} f(\mathbf{k}) \Omega(\mathbf{k})$, where $f(\mathbf{k})$ is the Fermi-Dirac distribution function, and the factor of 2 comes from spin degeneracy. There is also a side-jump contribution [23] proportional to the Berry curvature when carriers scatter off an impurity potential. The aforementioned symmetry argument manifests itself in the symmetry property of the Berry curvature $\Omega(\mathbf{k})$: it is an odd function in the presence of time reversal symmetry and even in the presence of inversion symmetry. From Eq. (1) we have for the conduction band

$$\Omega(\mathbf{q}) = \tau_z \frac{3a^2 \Delta t^2}{2(\Delta^2 + 3q^2 a^2 t^2)^{3/2}}. \quad (6)$$

Ignoring skew-scattering and other effects due to inter-valley scattering, we find a valley-dependent Hall conductivity as

$$\sigma_H(\tau_z) = \tau_z \frac{e^2}{h} \left[1 - \frac{\Delta}{2\mu} - \frac{3\Delta t^2 q_F^2 a^2}{8\mu^3} \right]. \quad (7)$$

where q_F is the Fermi wave vector which is related to the bulk chemical potential by $\mu = \frac{1}{2} \sqrt{\Delta^2 + 3q_F^2 a^2 t^2}$. The third term is the side-jump contribution, which is also independent of the scattering rate [24]. Interestingly, when the Fermi energy $\varepsilon_F = \mu$ is bigger than the gap Δ , such that the Berry curvature peak is well covered by occupied states, the Hall conductance approaches a quantized value of $\tau_z e^2/h$.

The valley dependence in the Hall current will lead to an accumulation of electrons on opposite sides of the sample with opposite valley index (see Fig. 2a). If an electric field E_y is applied along a strip of the sample, the valley population difference at one edge is given by

$$\delta n = j_x^v \tau_v = \sigma_H^v E_y \tau_v, \quad \sigma_H^v = \sum \tau_z \sigma_H(\tau_z)/e, \quad (8)$$

where τ_v is the inter-valley life time. The valley polarization is distributed along the edge within the diffusion length $l_F = v_F \sqrt{\tau_0 \tau_v}/2$, where v_F is the Fermi velocity and τ_0 is the intra-valley scattering time. From Ref. 4, we take $\tau_0 = 0.1$ ps and $\tau_v = 50$ ps. Assuming an electric field $E = 1$ mV/ μm , we find a valley population difference of 10 – 100 per μm along the edge and distributed over a width of $l_F \sim 1\mu\text{m}$. This valley polarization may be detected as a magnetic signal as we discussed before.

Clearly, if there is a net valley polarization ($\mu_1 \neq \mu_2$), a Hall current will appear upon the application of an electric field E_y ,

$$j_x = \frac{e^2}{h} \left[\frac{\Delta}{2\bar{\mu}^2} - \frac{9\Delta t^2 \bar{q}_F^2 a^2}{8\bar{\mu}^4} \right] \delta \mu E_y. \quad (9)$$

This Hall current will then lead to a measurable transverse voltage across the sample. If the width of the bulk region is smaller or comparable to the mean free path, the transverse voltage along the edge gives a local mapping of the valley polarization in the bulk. We show in Fig. 2b an experimental setup in conjunction with the valley filter device [5] to demonstrate this effect (we note that inversion symmetry breaking does not change the edge state property needed for the valley filter to function).

The valley magnetic moment and valley Hall effect predicted above are generic features in systems with broken inversion symmetry, as shown by another example, the biased bilayer graphene. This system may be modeled by an intra-layer nearest neighbor hopping t , an inter-layer nearest neighbor hopping t_\perp , and an energy bias Δ between the layers, which breaks the inversion symmetry [9]. Angle-resolved photoemission spectroscopy studies [8] of bilayer graphene films synthesized on SiC substrates confirm the band structure from this model.

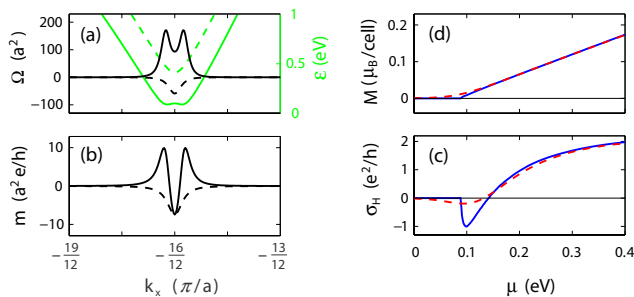


FIG. 3: (color online). Valley contrasting properties of conduction bands in biased graphene bilayer. (a) Energy dispersion (green or gray curves) and Berry curvature (black curves). (b) Orbital magnetic moment. Solid curves for lower conduction band and dashed curve for upper conduction band. The quantities are shown for the K_1 valley. Distributions of $m(\mathbf{k})$ and $\Omega(\mathbf{k})$ have opposite signs in the K_2 valley. The corresponding valley magnetization (c) and the valley Hall conductivity (d) are also shown as a function of chemical potential. The parameters used are $t = 2.82$ eV, $\Delta = 0.2$ eV, and $t_{\perp} = 0.4$ eV.

Biased bilayer graphene has two positive energy bands (conduction) and two negative energy bands (valence) if spin degeneracy is discounted. In Fig. 3, we show numerically calculated energy bands, Berry curvatures and orbital magnetic moments of the two conduction bands. The parameter values are chosen in accordance with experimental result [8]. $\Omega(\mathbf{k})$ and $m(\mathbf{k})$ are again peaked at the valley bottom. The valley magnetization and the valley Hall effect are of the same order of magnitude as in the epitaxial single-layer graphene. We note that the valley-dependent Hall conductance approaches a quantized value of $2\tau_z e^2/h$, twice of that for the single layer. This is consistent with the fact that in bilayer graphene, the Berry phase acquired by an electron during one circle around the valley becomes $\pm 2\pi$ instead of $\pm\pi$ when the gap closes [25].

The authors thank C.-K. Shih for discussions on the experimental aspect of measuring the valley Hall effect, A. Lanzara for sending us the manuscript before publication, and also acknowledge useful discussions with Y. Barlas, K. Nomura, and H. Min. This work is supported by NSF, DOE, and the Welch Foundation.

* These authors contributed equally to this work.

- [1] K. S. Novoselov, A. K. Geim, S. V. Morozov, D. Jiang, M. I. Katsnelson, I. V. Grigorieva, S. V. Dubonos, and A. A. Firsov, *Nature* **438**, 197 (2005); Y. Zhang, Y.-W. Tan, H. L. Stormer, and P. Kim, *Nature* **438**, 201 (2005).
 [2] A. K. Geim and K. S. Novoselov, *Nat. Mater.* **6**, 183

- (2007).
 [3] S. V. Morozov, K. S. Novoselov, M. I. Katsnelson, F. Schedin, L. A. Ponomarenko, D. Jiang, and A. K. Geim, *Phys. Rev. Lett.* **97**, 016801 (2006); A. F. Morpurgo and F. Guinea, *ibid.* **97**, 196804 (2006).
 [4] R. V. Gorbachev, F. V. Tikhonenko, A. S. Mayorov, D. W. Horsell, and A. K. Savchenko, *ibid.* **98**, 176805 (2007).
 [5] A. Rycerz, J. Tworzydło, and C. W. J. Beenakker, *Nature Phys.* **3**, 172 (2007).
 [6] S. Murakami, N. Nagaosa, and S.-C. Zhang, *Science* **301**, 1348 (2003); J. Sinova, D. Culcer, Q. Niu, N. A. Sinitsyn, T. Jungwirth, and A. H. MacDonald, *Phys. Rev. Lett.* **92**, 126603 (2004).
 [7] S. Y. Zhou, G.-H. Gweon, A. V. Fedorov, P. N. First, W. A. de Heer, D.-H. Lee, F. Guinea, A. H. C. Neto, and A. Lanzara, *Nat. Mater.*, in press.
 [8] T. Ohta, A. Bostwick, T. Seyller, K. Horn, and E. Rotenberg, *Science* **313**, 951 (2006).
 [9] E. McCann and V. I. Fal'ko, *Phys. Rev. Lett.* **96**, 086805 (2006); E. V. Castro, K. S. Novoselov, S. V. Morozov, N. M. R. Peres, J. M. B. Lopes dos Santos, J. Nilsson, F. Guinea, A. K. Geim, and A. H. Castro Neto, *cond-mat/0611342* (2006); H. Min, B. Sahu, S. K. Banerjee, and A. H. MacDonald, *Phys. Rev. B* **75**, 155115 (2007).
 [10] O. Gunawan, Y. P. Shkolnikov, K. Vakili, T. Gokmen, E. P. D. Poortere, and M. Shayegan, *Phys. Rev. Lett.* **97**, 186404 (2006).
 [11] G. Giovannetti, P. A. Khomyakov, G. Brocks, P. J. Kelly, and J. van den Brink, *arXiv:0704.1994* (2007).
 [12] G. W. Semenoff, *Phys. Rev. Lett.* **53**, 2449 (1984).
 [13] G. Sundaram, Ph.D. thesis, The University of Texas at Austin (2000).
 [14] C. L. Kane and E. J. Mele, *Phys. Rev. Lett.* **95**, 226801 (2005).
 [15] H. Min, J. E. Hill, N. A. Sinitsyn, B. R. Sahu, L. Kleinman, and A. H. MacDonald, *Phys. Rev. B* **74**, 165310 (2006); Y. Yao, F. Ye, X.-L. Qi, S.-C. Zhang, and Z. Fang, *Phys. Rev. B* **75**, 041401 (2007).
 [16] M.-C. Chang and Q. Niu, *Phys. Rev. B* **53**, 7010 (1996).
 [17] Y. Yafet, in *Solid State Physics: Advances in Research and Applications* (Academic Press, 1963), vol. 14.
 [18] L. L. Foldy and S. A. Wouthuysen, *Phys. Rev.* **78**, 29 (1949).
 [19] C.-P. Chuu, M.-C. Chang, and Q. Niu, unpublished.
 [20] D. Xiao, J. Shi, and Q. Niu, *Phys. Rev. Lett.* **95**, 137204 (2005); T. Thonhauser, D. Ceresoli, D. Vanderbilt, and R. Resta, *ibid.* **95**, 137205 (2005); D. Xiao, Y. Yao, Z. Fang, and Q. Niu, *ibid.* **97**, 026603 (2006).
 [21] R. Karplus and J. M. Luttinger, *Phys. Rev.* **95**, 1154 (1954).
 [22] T. Jungwirth, Q. Niu, and A. H. MacDonald, *Phys. Rev. Lett.* **88**, 207208 (2002).
 [23] L. Berger, *Phys. Rev. B* **2**, 4559 (1970).
 [24] N. A. Sinitsyn, Q. Niu, and A. H. MacDonald, *Phys. Rev. B* **73**, 075318 (2006).
 [25] K. S. Novoselov, E. McCann, S. V. Morozov, V. I. Fal'ko, M. I. Katsnelson, U. Zeitler, D. Jiang, F. Schedin, and A. K. Geim, *Nature Phys.* **2**, 177 (2006).